Dyes and Pigments 85 (2010) 109–116

Contents lists available at ScienceDirect

Dyes and Pigments

journal homepage: www.elsevier.com/locate/dyepig

Structural and spectroscopic characteristics of polycyclic fluorophores relevant to organic light-emitting diodes

Z. Liu*

Department of Chemistry, Hebei University of Engineering, Handan, 056038 Hebei, China

ARTICLE INFO

Article history:
Received 22 April 2009
Received in revised form
14 October 2009
Accepted 17 October 2009
Available online 28 October 2009

Keywords:
DFT
TDDFT
Polycyclic fluorophore
OLED
Excited state

ABSTRACT

Seminaphtho[a]-fluorone (SNAFR-1) and 7,8,10-triphenylfluoranthene (TPF), recently synthesized polycyclic fluorophores, are used in organic light-emitting diodes (OLEDs) as novel emitting layers. The electronic structures and spectroscopic properties of SNAFR-1 and TPF in the gas phase have been studied by the DFT/TDDFT methods using hybrid functionals, B3LYP and PBE0, and the 6-31G(d) basis set. The lowest singlet electronic transitions ($S_0 \rightarrow S_1$) in SNAFR-1 and TPF are delocalized over the whole molecules. On the basis of the CIS-optimized structure of the excited states, TD-PBE0 calculations predict emission wavelength of 572 nm for SNAFR-1, and of 475 nm for TPF, which are comparable, respectively, to 560 and 468 nm observed experimentally for photoluminescence.

1. Introduction

Organic light-emitting diodes (OLEDs) are of interest for the new generation of lighting applications, because of their unique features in lighting and flat-panel display technologies [1]. Compared with liquid crystal displays (LCDs), OLEDs are lighter, have a wider viewing angle, have a significantly lower cost, and can be made into flexible displays [2]. OLEDs seem to be the perfect technology for all types of displays, but they also have some disadvantages include (i) low external quantum efficiency [3], (ii) expensive and complicated manufacturing processes [4]. For example, white OLEDs, to date highly sought-after OLEDs, require multiemission layer structures, such as red, green, and blue fluorophores from different doped organic materials, to obtain white emission, and at least two precise controls of the dopant concentrations to obtain the color stability [5]. Since the first efficient OLEDs were obtained by Tang et al. in 1987 [6], remarkable advances have been made in improving the efficiencies of OLEDs, mainly including doped emitting layers [7], novel hole-transport materials [8], and efficient injection contacts [9]. Meanwhile much progress have been made in simplifying the manufacturing process by using dual doped structure [10], two emission zones [11], and fused organic solid solution [5]. In general, the key element of these multicomponent systems is the organic fluorophore used as a light emitter. During the last two decades, research advances in OLEDs are focusing almost entirely on the creative synthesis of new materials that can undergo efficient electroluminescence at a variety of wavelengths such as polymers [12], soluble octasubstituted metallophthalocyanines [13], novel organic salts [14,15], merocyanine dye aggregate [16], and oxystyryl dyes [17].

Recently, some novel organic fluorophores, with polycyclic rings, have been synthesized, such as a new seminaphtho[a]-fluorone (SNAFR-1) (see Fig. 1a) that can emit approximately equal intensities of blue, green and red light, via optimizing both solution parameters and excitation, and therefore serve as a simple white light-emitting fluorophore [18]; and 7,8,10-triphenylfluoranthene (TPF) (see Fig. 1b) that can be synthesized easily from cheap, commercially available materials, and emits blue light in a single-layer device architecture with very respectable efficiencies and low turn-on voltages [19]. It becomes clearer with time that, in order to make progress in the improvement of OLEDs, a deeper understanding is needed at the microscopic level. As a relatively new type of device, OLEDs are still largely unexplored in the aspect of the fundamental science underlying their functioning. Herein, we performed theoretical calculations on SNAFR-1 and TPF using density functional theory (DFT) methods. The results of this article are aimed at gaining insight into fundamental issues such as the electronic structures responsible for photoluminescence.

* Tel.: +86 310 8578796.
E-mail address: zliu_chem@live.cn

0143-7208/$ – see front matter © 2009 Elsevier Ltd. All rights reserved.
doi:10.1016/j.dyepig.2009.10.011

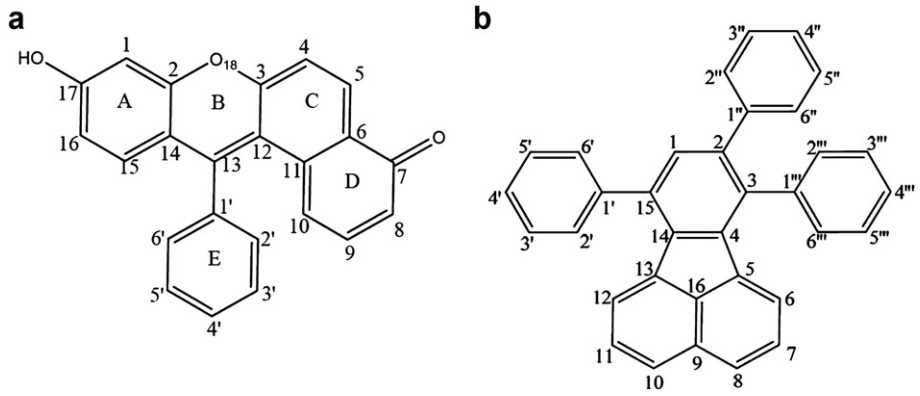

Fig. 1. Structure and atom numbering of (a) SNAFR-1, (b) TPF.

2. Computational details

The ground-state geometries of SNAFR-1 and TPF were optimized using the B3LYP/6-31G(d) method [20,21]. Based on the ground-state optimized geometries, the CIS/6-31G(d) method [22] was used to optimize the lowest singlet excited-state geometries for the two organic fluorophores. Since the TDDFT method provides a considerable improvement over CIS, even for small systems such as benzene [23], the vertical excitation energies and oscillator strengths have been then computed at the TD-PBE0 [24] level, by using standard 6-31G(d) basis set. In a recent literature [25] concerning functional assessment PBE0 has indeed proved its efficiency to evaluate the absorption spectrum of organic dyes. At stage of computing the absorption and emission spectra solvent effects were not taken into account. Concerning the reasons, we want to stress two points. First is the polycyclic systems under investigation in this paper. It is found that TDDFT approaches (B3LYP and BP86) underestimate the excitation energies for the lowest-lying single-t–singlet transition in polycyclic systems [26]. Second is the solvent effect. Conceptually, when the ground state of a fluorophore is preferentially stabilized by a solvent, which will increase the transition energy gap and induce a blue shift in the spectrum. In contrast, when the excited state is stabilized by a solvent and the transition energy decreases, which is observed as a red-shift in the spectrum. As for SNAFR-1 and TPF, our preliminary test calculations of excitation energies show that the degree of red-shift in solvent is more significant than that in vacuum. This is commonly true for organic dyes. Whereas, for metallorganic dyes, the inclusion of the solvent effect usually blue shifts λ_{max} with respect to the gas phase. So for SNAFR-1 and TPF the results in vacuum could be better to describe the spectral features. From Table 3 in Section 3.2 we can see that TD-PBE0 rightly reproduced the experimental absorption and emission maxima. All of the calculations were accomplished by using the Gaussian 03 software package [27].

3. Results and discussion

3.1. Ground- and excited-state geometries

3.1.1. Seminaphtho[a]-fluorone (SNAFR-1)

SNAFR-1 exists in the cationic and neutral form depending on the pH of the solutions [18]. Molecular structure of neutral SNAFR-1 was described herein. The main optimized ground- and lowest singlet excited-state geometry structural parameters for SNAFR-1 are presented in Table 1, and the optimized geometry in the ground state is shown in Fig. 2a. The molecule can be divided into two fragments of chemical significance: the 4-fused ring system (A-, B-, C- and D-rings), and the phenyl ring (E-ring). SNAFR-1 has a noticeable nonplanar conformation, mainly as a result of the steric crowding of the four hydrogen atoms that attach to $C_{2'}$, $C_{6'}$, C_{10} and C_{15}, which will bring a obstacle against free rotation of the phenyl. One can expect that both structure and photophysical behavior of SNAFR-1 should be determined mainly by the spatial orientations. The fused ring also shows an obviously distorted conformation for both structures. The C_8, C_9, C_{10} and C_{11} atoms have the largest deviation from the mean plane of the fused ring, and the torsion

Table 1
The main optimized bond lengths, angles and dihedral angles of the S_0 ground state (calculated by B3LYP method) and S_1 excited state (CIS method) of SNAFR-1.

	S_0	S_1	% diff[a]
	B3LYP/6-31G(d)	CIS/6-31G(d)	
Bond lengths (±0.001 Å)			
C_1–C_2	1.418	1.391	−1.90
C_2–O_{18}	1.362	1.389	1.98
O_{18}–C_3	1.367	1.402	2.56
C_3–C_4	1.374	1.336	−2.76
C_4–C_5	1.450	1.447	−0.20
C_5–C_6	1.371	1.349	−1.60
C_6–C_7	1.502	1.465	−2.46
C_7–C_8	1.493	1.446	−3.15
C_8–C_9	1.355	1.338	−1.25
C_9–C_{10}	1.458	1.450	−0.55
C_{10}–C_{11}	1.371	1.347	−1.75
C_{11}–C_{12}	1.484	1.503	1.28
C_{12}–C_{13}	1.381	1.347	−2.46
C_{13}–C_{14}	1.477	1.488	0.74
C_{14}–C_{15}	1.419	1.397	−1.55
C_{15}–C_{16}	1.397	1.378	−1.36
C_{16}–C_{17}	1.425	1.398	−1.89
C_{17}–C_1	1.415	1.389	−1.84
C_2–C_{14}	1.432	1.401	−2.16
C_3–C_{12}	1.487	1.490	0.20
C_6–C_{11}	1.487	1.483	−0.27
$C_{1'}$–C_{13}	1.489	1.514	1.68
$C_{1'}$–$C_{2'}$	1.416	1.394	−1.55
$C_{2'}$–$C_{3'}$	1.406	1.386	−1.42
Bond angles (±0.1°)			
C_6–C_5–H	122.1	120.9	
C_7–C_8–H	117.7	118.2	
C_9–C_{10}–H	115.7	116.6	
C_{16}–C_{15}–H	117.4	118.9	
C_{17}–C_{16}–H	120.8	119.8	
C_9–C_8–H	121.7	122.4	
Dihedral angles (±0.1°)			
C_8–C_7–C_6–O_{11}	−23.6	−6.5	
C_{10}–C_{11}–C_{12}–C_{13}	−37.6	−20.9	
C_{11}–C_{12}–C_3–C_4	20.4	13.6	
C_{13}–C_{12}–C_3–O_{18}	21.6	16.3	

[a] % difference defined as $((R_{CIS} - R_{B3LYP})/R_{CIS}) \times 100\%$.

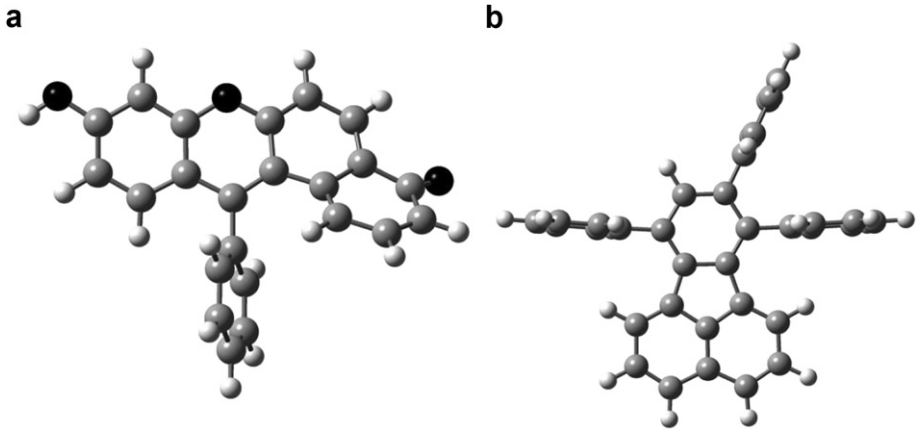

Fig. 2. Optimized structures of (a) SNAFR-1, (b) TPF in the gas phase, calculated at B3LYP/6-31G(d) level.

angle C_{10}–C_{11}–C_{12}–C_{13} of the S_0 state is −37.6°. Obviously, the 4-fused ring system bearing one phenyl substituent is generally rigid, which is usually important for light-emitting materials since the conformational changes resulted from the rotation of substitute groups may lead to a non-radiating transition. Optimization by the CIS method of the S_1 state of SNAFR-1 starting from the nonplanar initial geometry produced a more planar structure; and the torsion angle C_{10}–C_{11}–C_{12}–C_{13} of the S_1 state is −20.9°.

The changes in bond length along the CC conjugation due to singlet excitation in SNAFR-1 are shown in Table 1. In the excited S_1 state, all the bond lengths of the A-ring and the E-ring decrease, whereas the bond length of $C_{1'}$–C_{13} that connects the E-ring to the B-ring, most of the B-ring bond lengths, and all the CO bond lengths increase. The geometric changes in SNAFR-1 due to excitation are significant along almost the entire carbon backbone. The increase in the CC bond length is on the order of 0.02 Å for the singlet, and the maximum decrease of the CC bond length is on the order of 0.04 Å. The delocalization of the bond length changes along the carbon backbone of the molecule, indicating that the lowest singlet excitation of the molecule is also delocalized.

The bond length alternation (BLA) along the CC conjugation length due to singlet excitations in SNAFR-1 was also estimated, which reflects an uneven distribution of the π electrons over the bonds and is therefore strongly coupled to the electronic system. The significant alternating CC bond lengths of SNAFR-1 was observed, in both S_0 and S_1 states, along 11-carbon-atoms length C_7–C_8–C_9–C_{10}–C_{11}–C_{12}–C_{13}–C_{14}–C_{15}–C_{16}–C_{17}. It is also noticed that, although the π-system is extended, there is an alternation of the π-bond lengths inside the phenol aromatic ring (A-ring) of SNAFR-1 in both states. Starting from the C_2–C_1 bond of the A-ring, the bond lengths are 1.418 (C_2–C_1), 1.415 (C_1–C_{17}), 1.425 (C_{17}–C_{16}), 1.397 (C_{16}–C_{15}), 1.419 Å (C_{15}–C_{14}) for the S_0 state, and the corresponding values for the S_1 state are 1.391, 1.389, 1.398, 1.378, 1.397 Å. Such a phenomenon is not observed in the phenyl ring (E-ring) of SNAFR-1. The bond length alternation in benzene anneleated to small rings has long been observed and originally attributed to the so-called Mills–Nixon effect [28]. However, recent studies oppose using the Mills–Nixon effect for these kinds of phenomena [29]. Anyway, in most cases of the fused systems, bond elongation or contraction can arise, and the fusion leads to a decrease in aromaticity [30]. Resulting from symmetry of SNAFR-1 distorted, π-bond lengths alternate, as they do in linear conjugated chains. Consequently, by the geometric criterion, SNAFR-1 in either state is of low aromatic. But the A- and E-rings should maintain the aromatic character, because the benzene ring can suffer significant BLA and distorted ring geometry without a substantial loss of its cyclic electron delocalization and its aromaticity [31].

These changes in the geometry due to excitation can be explained using the ESF theory proposed by Nakatsuji [32]. In ESF theory, the geometric changes in the excited state can be explained by the force acting on nuclei caused by changes in the electron distribution. To account for the geometry changes caused by excitation in SNAFR-1, the difference in electron density between the ground state and the lowest singlet excited state is also investigated. The change in electron density due to excitation is pronounced, as is apparent from Fig. 3a. In the case of singlet

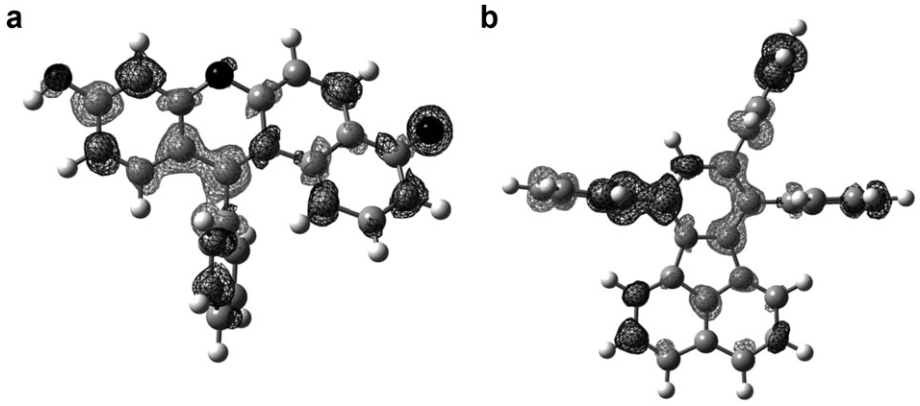

Fig. 3. Density difference between the first excited state and the ground state for (a) SNAFR-1, (b) TPF. The darker (black) color shows increased electron density in the excited state and the lighter (grey) color shows decreased electron density relative to the ground state.

Table 2
The main optimized bond lengths, angles and dihedral angles of the S_0 ground state (calculated by B3LYP method) and S_1 excited state (CIS method) of TPF.

	S_0	S_1	% diff[a]
	B3LYP/6-31G(d)	CIS/6-31G(d)	
Bond lengths (±0.001 Å)			
C_1–C_2	1.404	1.456	3.70
C_2–C_3	1.435	1.362	−5.09
C_3–C_4	1.406	1.437	2.20
C_4–C_5	1.486	1.412	−4.98
C_5–C_6	1.384	1.410	1.88
C_6–C_7	1.437	1.386	−3.55
C_7–C_8	1.386	1.396	0.72
C_8–C_9	1.439	1.412	−1.88
C_9–C_{10}	1.439	1.409	−2.08
C_{10}–C_{11}	1.386	1.400	1.01
C_{11}–C_{12}	1.437	1.382	−3.83
C_{12}–C_{13}	1.383	1.413	2.17
C_{13}–C_{14}	1.482	1.406	−5.13
C_{14}–C_{15}	1.401	1.440	2.78
C_{15}–C_1	1.423	1.353	−4.92
C_{15}–$C_{1'}$	1.487	1.515	1.88
C_2–$C_{1''}$	1.491	1.516	1.68
C_3–$C_{1'''}$	1.489	1.516	1.81
Bond angles (±0.1°)			
C_{15}–C_1–H	118.2	119.7	
C_6–C_7–H	117.7	118.2	
C_{10}–C_{11}–H	119.7	117.7	
C_{13}–C_{12}–H	122.9	121.3	
C_{16}–C_5–C_6	117.3	117.3	
C_{12}–C_{13}–C_{16}	117.7	117.4	
Dihedral angles (±0.1°)			
C_{14}–C_{15}–$C_{1'}$–$C_{2'}$	91.1	90.6	
C_1–C_2–$C_{1''}$–$C_{2''}$	−89.1	−89.0	
C_4–C_3–$C_{1'''}$–$C_{6'''}$	−90.1	−89.9	
C_{13}–C_{14}–C_4–C_5	0.0	0.0	

[a] % difference defined as $((R_{CIS} - R_{B3LYP})/R_{CIS}) \times 100\%$.

excitation, the electron distribution changes in the vicinity of some C nuclei, as seen in the figure. These accumulations (depletions) of electron density are manifested by changes in the corresponding CCC or CCH angles. For example, angle C_{16}–C_{15}–H is enlarged in the singlet excited state (118.9°) from that in the ground state (117.4°) as a result of an accumulation of electron density in the region of the associated C nucleus. On the other hand, angle C_{17}–C_{16}–H is narrowed by 1.0°, from 120.8 to 119.8°, as a result of excitation as electron density depleted in the region of the associated C nucleus. Similar arguments can apply to the other bond angle changes in SNAFR-1 by comparing the ground- and excited-state electron densities.

3.1.2. 7,8,10-Triphenylfluoranthene (TPF)

We performed full optimization for the S_0 and S_1 states and obtained stable geometries very close to C_s symmetry. Table 2 and Fig. 2b report the ground- and excited-state geometry structural parameters and the optimized geometry in the ground state of TPF, respectively. The molecule can be divided into two fragments of chemical significance: the fluoranthene ring, and the three phenyl arms. These groups are rather rigid, favoring light-emitting characteristics, due to the spatial repulsion of the hydrogen atoms in *peri*-positions. For the S_0 state of TPF, the molecule is twisted around the $C_{1'}$–C_{15}, the C_2–$C_{1''}$, and the C_3–$C_{1'''}$ bonds by 91.1, −89.1 and −90.1°, respectively. The corresponding values for the S_1 state are 90.6, −89.0 and −89.9°, respectively. In each case, although the atoms of the fluoranthene moiety are completely coplanar, the molecule is disordered in positions C_5 and C_{13} that are in the naphthalene framework from the five-membered ring. Angles C_{12}–C_{13}–C_{16} and C_{16}–C_5–C_6, deviating from 120°, in the S_0 state are 117.7 and 117.3°, respectively; while those of the corresponding angles in the S_1 state are 117.4 and 117.3°, respectively. The changes in bond length along the CC conjugation due to singlet excitation in TPF are shown in Table 2. In the lowest excited states, the increase of CC bond length is localized within the fluoranthene moiety of the molecule. The CC bonds that connect the three phenyl rings to the fluoranthene ring are all elongated by as much as around 0.03 Å. While the bond length of CC bonds in the three phenyl rings reduces by as much as around 0.02 Å. The highest changes occur for the CC bonds in the fluoranthene ring, which decrease and increase by 0.08 and 0.05 Å, respectively; indicating that the lowest singlet excitations of the molecule is mainly localized in the fluoranthene moiety. In the excited state, the single bonds (C_4–C_5 and C_{13}–C_{14}) joining the benzene and the naphthalene rings in the fluoranthene moiety have acquired a certain amount of aromatic-bond character (the typical aromatic-bond length is 1.40 Å), and the inter-ring structure is forced into a completely planar structure, as is clear from Table 2 (see the bond lengths and dihedral angles related to the five-membered ring).

Although the π-system is extended, there is an alternation of the aromatic-bond lengths inside the fluoranthene ring, and such a phenomenon is already reported for acenaphthylene, the precursor of fluoranthene, by a theoretical study [33]. In the S_0 state, all the aromatic bonds of the benzene and the naphthalene rings in the fluoranthene moiety exhibit distinct alterations in bond lengths, and as that of SNAFR-1, the difference in lengths between the long and short bonds varies. While in the S_1 state only half amount of the aromatic bonds display BLA with reduced degree of bond alternation, indicating that the ring–ring repulsions of TPF

Table 3
Excitation energies (ΔE) and oscillator strengths (*f*) for SNAFR-1 (HOMO is MO 88) and TPF (HOMO is MO 113).

Transition	TD-PBE0/6-31G(d)			Experiment [18,19]	
	Configuration	ΔE/eV (nm)	*f*	ΔE/eV (nm)	Intensity (M^{-1} cm^{-1})
The absorption of SNAFR-1					
$X^1A \rightarrow A^1A$	0.13(87a–89a) + 0.58(88a–89a)	2.26 (550)	0.355	2.35(528)	6000
$X^1A \rightarrow B^1A$	0.65(87a–89a) + 0.11(87a–90a) − 0.12(88a–89a)	2.68 (463)	0.042	2.52(493)	7500
The emission of SNAFR-1					
$A^1A \rightarrow X^1A$	0.57(89a–87a) + 0.12(90a–87a) − 0.30(89a–88a)	2.17 (572)	0.078	2.22 (560)	
The absorption of TPF					
$X^1A \rightarrow A^1A$	−0.12(110a–114a) + 0.66(112a–114a)	3.43 (362)	0.011	3.29 (377)	10 000
$X^1A \rightarrow B^1A$	−0.21(112a–115a) + 0.63(113a–114a)	3.63 (342)	0.230	3.75 (331)	8800
$X^1A \rightarrow C^1A$	0.12(109a–114a) + 0.55(110a–114a) −0.27(113a–115a) + 0.20(113a–116a) +0.20(113a–120a)	4.24 (292)	0.057	4.18 (297)	32 000
The emission of TPF					
$A^1A \rightarrow X^1A$	0.66(114a–113a) + 0.10(114a–108a)	2.61 (475)	0.015	2.65 (468)	80 000

decrease due to the elongated bonds connecting the phenyl and the fluoranthene rings. Likewise, the aromatic rings in the fluoranthene moiety should maintain the aromatic character in despite of the geometric structures displaying BLA, by the same reason as for SNAFR-1 [31]. No such BLA phenomenon is observed in any phenyl arm. The differences in electron density between the ground and lowest singlet excited state due to excitation in TPF is shown in Fig. 3b. The geometry changes in TPF can also be explained by ESF theory, as described in the previous subsection for SNAFR-1.

3.2. Absorption and emission spectra

3.2.1. Seminaphtho[a]-fluorone (SNAFR-1)

The CIS method for excited states can be compared to Hartree–Fock theory for the ground state. More accurate methods such as multireference methods would be desirable, but these are too expensive for the large molecules. The TDDFT method provides a cost-effective alternative to multireference ab initio methods, performs well for valence excited states and can be applied to quite large systems [34,35]. The vertical excitation energies from the ground state to singlet excited states were calculated by the TD-PBE0/6-31G(d) method using the B3LYP/6-31G(d) optimized ground-state geometry. Table 3 presents the vertical excitation energies, the corresponding maximum absorption wavelengths, oscillator strengths and the experimental values [18]. Two energetically close pairs of orbitals, the two highest occupied molecular orbitals (HOMO and HOMO-1) and the two lowest virtual MOs (LUMO and LUMO+1), are involved in the lowest singlet transition. The main configuration of the A^1A state, which corresponds to the first excited state is the HOMO → LUMO excitation, as in most π-conjugated systems. The main configuration of the B^1A state, which correspond to the second excited state is mainly contributed by the HOMO-1 → LUMO excitation. In comparison with experimental absorption intensities, the calculated oscillator strengths (*f*) of the dipole-allowed do not give the experimental ordering of the singlet–singlet transition strengths in SNAFR-1. This discrepancy suggests that there are other factors than dipole transition moments that determine the absorption strength, such as vibrational effects. It is predicted that the lowest energy absorption maximum observed in the spectral experiments originates in the A^1A state. The calculated λ_{max} value is in good agreement with experimental result, with the deviation being 22 nm (0.09 eV). Form the theoretical point, the result gives credit to the DFT approach, and appropriate absorption spectra may be reproduced with good accuracy for organic dyes with fused aromatic rings.

We now turn our attention to the electronic structure of the frontier orbitals. To understand the excitation in SNAFR-1 better, it is necessary to look at the molecular orbitals involved in the transition. As expected, in both cases, the HOMO and LUMO orbitals have π character (see Fig. 4). The π orbitals are delocalized within the 4-fused ring moiety (A-, B-, C- and D-rings), and the conjugation between the C- and the D-rings can be seen clearly. The delocalization region of the orbitals from the HOMO to LUMO are almost identical. Minor differences may be pointed out. The HOMO orbital has more amplitude on the A- and B-rings and less on the D-ring, compared with the LUMO. Both the HOMO and LUMO orbitals have almost no amplitude on the E-ring. While the HOMO-1, 0.88 eV below the HOMO, is almost localized within the D-ring, of sigma character on the carbon atoms and π character on the oxygen atom. One of the key questions to be addressed is whether the excitations in the large system such as SNAFR-1 are localized on a fragment or delocalized over the whole molecule. The question of localized versus delocalized transitions in the absorption spectra can be addressed by examining the total electron density difference between the ground state and the excited state. Fig. 3a shows the density difference plots for the lowest excitation ($S_0 \rightarrow S_1$) of SNAFR-1. The isodensity value shown in the figure is 0.00001 e/bohr^3. When the isodensity value is increased to 0.0001, no

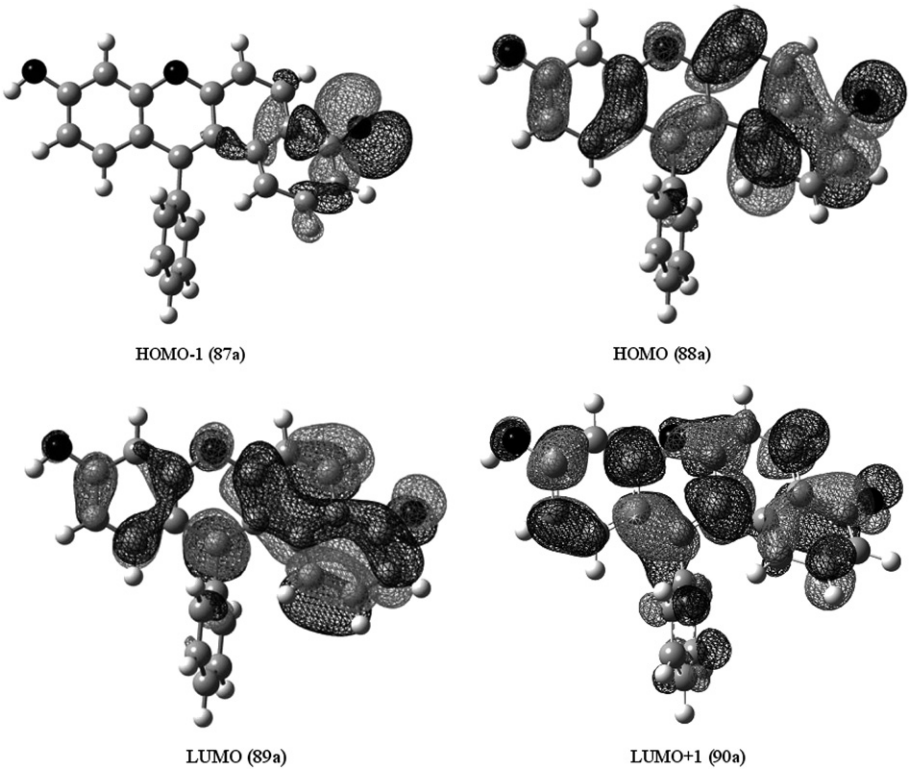

Fig. 4. The molecular orbitals of SNAFR-1.

surfaces are seen in the electron density difference plot, indicating that the amount of charge redistributed must be less than 0.0001 e/bohr^3. The similar shapes of the HOMO and LUMO orbitals result in the small charge redistribution. The delocalized nature of the excitation in the molecule can be clearly seen from this figure. The present electronic structure calculations indicate that lowest vertical excitation for SNAFR-1 is not localized to individual aromatic units but is fully delocalized over the entire molecule.

At the basis of the optimized excited singlet-state geometry at the CIS level, TD-PBE0/6-31G(d) is used to calculate the emission spectra. Table 3 displays experimental and calculated emission energies for SNAFR-1 as well as their corresponding computed oscillator strengths. Since SNAFR-1 is a single component red-green-blue (RGB) fluorophore, experimentally, this molecule emits in the violet-blue, green, and red spectral regions. The green emission is attributed to the neutral SNAFR-1 under investigation in this paper [18]. A small shift (0.09 eV/22 nm) is observed between the optical absorption spectra and emission spectra, thought to arise from slight differences between the ground- and excited-state structures. The lowest energy singlet transition mainly involves transitions from the lowest energy LUMO orbital, 89a, to the highest and the second highest energy HOMO orbitals, 88a and 87a, with more weight on the transition (89a → 87a). The difference between the calculated absorption and emission wavelengths, 22 nm, can be compared to the experimental Stokes shift of 32 nm for SNAFR-1 in DMSO [18]. Furthermore, that TD-PBE0 calculations yield a vertical excitation energy of 2.17 eV (572 nm) for the emission indicates that PBE0 is able to deliver reasonable estimates of the color of organic dyes with fused aromatic rings.

3.2.2. 7,8,10-Triphenylfluoranthene (TPF)

The vertical excitation energies for the lowest singlet transitions calculated by the TD-PBE0 method, their oscillator strengths, and the main configurations as well as the experimental results [19] are collected in Table 3. The TD-PBE0/6-31G(d) calculation shows the presence of three states at 3.43 (362 nm), 3.63 (342 nm) and 4.24 eV (292 nm) with oscillator strengths (f) of 0.011, 0.230 and 0.057, respectively. The calculated spectrum quantitatively agrees with the experimental spectrum in CH_2Cl_2 which shows the bands at 3.29 eV (377 nm), 3.75 (331 nm) and 4.18 eV (297 nm). For the lowest-lying absorption, the deviation between theory and experiment is 15 nm (0.14 eV). Once again, TD-PBE0 provides a reliable description of the vertical excitation energies for the polycyclic system. Note that the TD-PBE0 calculations predict additional singlet transitions that are, however, too weak to be observed or lie outside the observation range, and hence they do not manifest themselves in the experimental spectrum. On the other hand, the molecule is very rigid and no thermal motion could cause sufficient distortion for these transitions to pick up some intensity in TPF. However one must keep in mind that the TDDFT method is found to underestimate the oscillator strength by about 30% lower than the experimental value even in a small system like benzene [36]. Like SNAFR-1, the calculated oscillator strengths (f) do not give the experimental ordering of absorption intensities of TPF. It should also suggest that additional parameters, like vibrational effects could determine the absorption strength of TPF, other than dipole transition moments. Table 3 shows that excitation of HOMO-1 (MO 112a) → LUMO (MO 114a) with the configuration coefficient of 0.66 is principally responsible for the 3.43 eV (362 nm) absorption band. While the other two bands at 3.63 eV (342 nm) and 4.24 eV (292 nm) are mainly HOMO (MO 113a) → LUMO (MO 114a) and HOMO-3 (MO 110a) → LUMO (MO 114a) in character, respectively. Note that several nearby molecular orbitals also contribute to a certain extent to the three absorption peaks.

The main molecular orbitals involved in the singlet transitions are shown in Fig. 5. The interpretation of spectral features is greatly assisted by detailed description of molecular orbitals, including spatial characteristics, nodal patterns, and individual atom contributions. As seen from Fig. 5, from the HOMO-1 to LUMO, the characteristic shapes of these orbitals are almost identical. All three orbitals are well localized within the fluoranthene moiety. Minor differences may be pointed out. The limited differences are; firstly, in the number and position of their internuclear nodal planes and, secondly, in the different amplitude on the phenyl arms. The HOMO-1 orbital (MO 112a) has small amplitude on one phenyl arm, the HOMO orbital (MO 113a) has very small amplitude on all three phenyl arms, the LUMO orbital (MO 114a) has almost no amplitude on any phenyl arms, but very small amplitude on two carbon atoms of one phenyl arm. In contrast, the HOMO-3 orbital (MO 110a) has a different shape with significant amplitude on two phenyl arms while almost no amplitude on the benzene ring of the fluoranthene moiety. Whereas the delocalized nature of the LUMO+1 (MO 115a) is clear, with almost whole molecule having significant amplitude. The observed geometry relaxation in TPF can be rationalized by consideration of the nodal patterns of the HOMO-1 and LUMO orbitals in Fig. 5. The $S_0 \rightarrow S_1$ excitation with the second large oscillator strength ($f = 0.011$) is mainly HOMO-1 → LUMO in character. For example, The LUMO (MO 114a) has a node across the C_{15}–C_{14}, but the HOMO-1 (MO 112a) is bonding in the region (see Figs. 1b and 5). Therefore one would expect elongation of the bond; Table 2 shows that the bond are in fact longer in the excited state. The HOMO-1 (MO 112a) has a node across the C_{14}–C_{13} bond while the LUMO (MO 114a) is bonding. The datum in Table 2 confirms the anticipated contraction of these bond. The other geometry changes can be rationalized from the similar argument.

The site of the electronic excitation can be readily identified by considering the difference in total electron density between the excited and ground states. As shown from the total electron density difference (see Fig. 3b), in despite of the localized nature of the molecular orbitals (HOMO-1 and LUMO), the lowest vertical excitations for TPF are not localized to the individual fluoranthene unit but are fully delocalized over the entire molecule. The characteristics of delocalization are attributed to the total electron transfers from the ground state (S_0) to the first excited state (S_1), not just the transitions with large contributions. As seen from Table 3, the theoretical spectrum has been blue shifted by 0.14 eV (15 nm) to match the experimental lowest-lying absorption 3.29 eV (377 nm). In addition to the improvement of PBE0 over B3LYP and BP86 red-shift error, one would expect that this is also a manifestation of a different extent of electron delocalization seen in TPF between the gas phase and solution phase.

We employed the CIS method to optimize the lowest singlet-state geometry, and at the excited singlet-state geometry, TD-PBE0/6-31G(d) was used to calculate the emission spectrum. The calculated fluorescence emission in the gas phase together with the experimental value in the solid state are given in Table 3. The photoluminescence for TPF corresponds to the lowest singlet S_1, which consists of the transition from HOMO to LUMO and from HOMO-5 to LUMO. The emission is calculated to be 475 nm (2.61 eV) which, as with the predicted absorption energy, is excellent agreement with the energy of the experimental photoluminescence emission observed in the solid state at 468 nm (2.65 eV) and the electroluminescence emission observed in devices at 480 nm (2.59 eV) [19]. The agreement between computation and experiment indicates that PBE0 is able to deliver reasonable estimates of the color of polycyclic system. It can be seen from these results that TPF has large stokes shifts of 113 nm. This large Stokes shift is assumed to be the consequence of a large structural change of fluoranthene moiety from the equilibrium

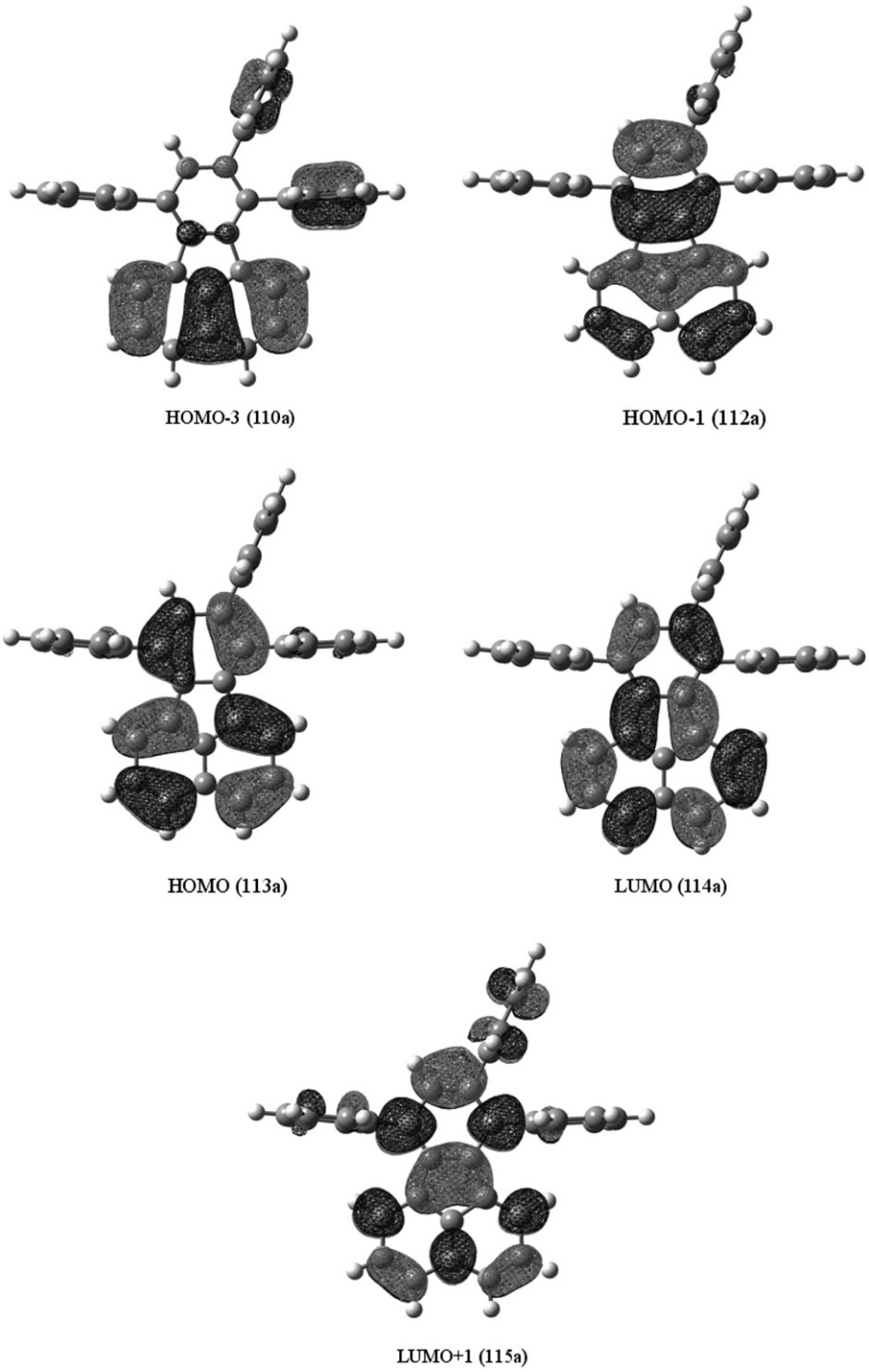

Fig. 5. The molecular orbitals of TPF.

ground-state geometry to the S_1 state equilibrium. Because the present calculations show that the excitation in TPF is primarily delocalized transition involving electron transfer from the HOMO to the LUMO, which have significant contributions from the fluoranthene atoms.

4. Conclusions

Electronic spectra and ground- and low-lying excited-state geometries of the OLED Materials SNAFR-1 and TPF, recently synthesized polycyclic fluorophores, were investigated using the DFT/TDDFT methods. We discussed geometry relaxations in detail. The changes in bond length due to excitation in SNAFR-1 are delocalized along the carbon backbone of the molecule, while in TPF, the bond length changes were found to be mainly localized in the fluoranthene moiety. The electronic structures have been discussed completely. The electronic excitation and the structural relaxation in the excited state for SNAFR-1 and for TPF have been interpreted in terms of the nature and nodal characteristics of the HOMO and LUMO, and HOMO-1 and LUMO, respectively. The $S_0 \rightarrow S_1$ excitations are found to be delocalized over the whole system for both the molecules studied as evidenced by the

structural shifts and the total electron density differences between the excited and ground electronic states. We conclude that the TD-PBE0 method at the CIS minimum energy geometry describes the spectroscopic properties of SNAFR-1 and TPF in the gas phase, both transition energies and oscillator strengths, reasonably well. By using the CIS/TDDFT methods most important spectral features, both transition energies and oscillator of both the molecules could be predicted. In our judgment the CIS/TDDFT methods are useful and computationally economical methods for the study of spectroscopic properties of rigid polycyclic systems.

References

[1] Forrest SR. Org Electron 2003;4:45–8.
[2] Pardo DA, Jabbour GE, Peyghambarian N. Adv Mater 2000;12:1249–52.
[3] Huang Q, Li J, Marks TJ, Evmenenko GA, Dutta P. J Appl Phys 2007;101:093101–13.
[4] Shao Y, Yang Y. Adv Funct Mater 2005;15:1781–6.
[5] Shao Y, Yang Y. Appl Phys Lett 2005;86:073510–3.
[6] Tang CW, VanSlyke SA. Appl Phys Lett 1987;51:913–5.
[7] Tang CW, VanSlyke SA, Chen CH. J Appl Phys 1989;65:3610–6.
[8] Ma CQ, Zhang LQ, Zhou JH, Wang XS, Zhang BW, Cao Y, et al. J Mater Chem 2002;12:3481–6.
[9] VanSlyke SA, Chen CH, Tang CW. Appl Phys Lett 1996;69:2160–2.
[10] Huang YS, Jou JH, Weng WK, Liu JM. Appl Phys Lett 2002;80:2782–4.
[11] Kim CH, Shinar J. Appl Phys Lett 2002;80:2201–3.
[12] Kippelen B, Meerholz K, Peyghambarian N. In: Nalwa HS, Miyata S, editors. Nonlinear Optics of organic molecules and polymers. Boca Raton: CRC Press; 1997. p. 465–513.
[13] Díaz-García MA, Ledoux I, Duro JA, Torres T, Agulló-López F, Zyss J. J Phys Chem 1994;98:8761–4.
[14] Kolev T, Koleva BB, Spiteller M, Mayer-Figge H, Sheldrick WS. Dyes Pigm 2008;79(1):7–13.
[15] Kolev T, Tsanev T, Kotov S, Mayer-Figge H, Spiteller M, Sheldrick WS, et al. Dyes Pigm 2009;82:95–101.
[16] Kolev T, Koleva BB, Stoyanov S, Spiteller M, Petkov I. Spectrochim Acta 70 A 2008:1087–96.
[17] Koleva BB, Stoyanov S, Kolev T, Petkov I, Spiteller M. Spectrochim. Acta 2009;71A:1857–64.
[18] Yang Y, Lowry M, Schowalter CM, Fakayode SO, Escobedo JO, Xu X, Zhang H, Jensen TJ, Fronczek FR, Warner IM, Strongin RM. J Am Chem Soc 2006;128:14081–92.
[19] Chiechi RC, Tseng RJ, Marchioni F, Yang Y, Wudl F. Adv Mater 2006;18:325–8.
[20] Becke AD. J Chem Phys 1993;98:5648–52.
[21] Lee C, Yang W, Parr RG. Phys Rev B 1988;37:785–9.
[22] Del Bene JE, Ditchfield R, Pople JA. J Chem Phys 1971;55:2236–41.
[23] Stratmann RE, Scuseria GE, Frisch MJ. J Chem Phys 1998;109:8218–24.
[24] Adamo C, Barone V. J Chem Phys 1999;110:6158–70.
[25] Jacquemin D, Perpète EA, Scuseria GE, Ciofini I, Adamo C. J Chem Theory Comput 2008;4:123–35.
[26] Parac M, Grimme S. Chem Phys 2003;292:11–21.
[27] Frisch MJ, Trucks GW, Schlegel HB, Scuseria GE, Robb MA, Cheeseman JR, et al. Gaussian 03, Revision B.01. Wallingford, CT: Gaussian, Inc.; 2004.
[28] Mills WH, Nixon IG. J Chem Soc 1930:2510–24.
[29] Stanger A. J Am Chem Soc 1998;120:12034–40.
[30] Krygowski TM, Cyrański MK. Chem Rev 2001;101(5):1385–420.
[31] Feixas F, Matito E, Poater J, Solá M. J Phys Chem A 2007;111:4513–21.
[32] Nakatsuji H. J Am Chem Soc 1973;95:345–54.
[33] Wang D, Violi A. J Org Chem 2006;71:8365–71.
[34] Dreuw A, Dunietz BD, Head-Gordon M. J Am Chem Soc 2002;124:12070–1.
[35] Dreuw A, Fleming GR, Head-Gordon M. J Phys Chem B 2003;107:6500–3.
[36] Matsuzawa NN, Ishitani A, Dixon D, Uda T. J Phys Chem A 2001;105:4953–62.